Destination Accessibility of a Hopping Robot on Small Celestial Bodies in Microgravity

*Keita Kobashi[1], Toshiyasu Kaneko[1], Kenji Nagaoka[1], and Kazuya Yoshida[1]

[1] *Tohoku University, Aoba 6-6-01, Aramaki, Aoba-ku, Sendai, Japan*
E-mail: {kobashi, kaneko, nagaoka, yoshida}@astro.mech.tohoku.ac.jp

ABSTRACT

Hopping mobility is effective for the use of an exploration robot on small celestial bodies such as asteroids and comets. However, the rebounding dynamics in such a case is influenced by non-uniform gravity and the surface shape of the body. Therefore, it is challenging for the robot to access its destination. This paper presents various movements of robots using hopping mobility. Moreover, this paper also presents the destination accessibility of such robots. In order to analyze the various movements of the robots, we focused on the hopping and rebounding motion of the robot. First, we modeled the hopping motion and rebounding motion, respectively, using the contact force model and linear springs and dampers. Second, we verified the hopping model through experiments in a 2D microgravity environment. Finally, we performed a dynamic simulation of the rebounding. The results showed that the characteristics of the rebounding motion are related to the hopping motion and that the characteristics can be significantly adjusted by altering the rebounding attitude and angular velocity of the robot. Based on this result, the destination accessibility is evaluated by using the following four characteristics, (1) moving accuracy, (2) traveling time, (3) energy efficiency, and (4) ability to leap over obstacles. This paper presents the conditions of hopping and rebounding motion that these four evaluation elements of destination accessibility emerge noticeably.

1 INTRODUCTION

There are several small bodies in our solar system. Small bodies such as asteroids and comets contain information regarding the origin of the solar system. However, the detailed composition of asteroids is unknown. Therefore, the exploration of asteroids for clarifying their composition is of great importance for revealing information regarding the origin of the solar system. Increasing attention has been focused on the exploration of small celestial bodies in recent years.

In 2010, Hayabusa [1, 2], an asteroid explorer developed by The Japan Aerospace Exploration Agency (JAXA), succeeded in its mission of collecting a sample from an asteroid called "Itokawa". Asteroids can be classified into several types based on their emission spectrum and their orbit, and Itokawa is classified as an S-type asteroid. This mission revealed the composition of S-type asteroids. To obtain more information regarding asteroids, asteroid-surface exploration is required. In general, exploration robots that can traverse an asteroid surface play a crucial role in asteroid-surface exploration. In the case of Mars exploration, the dynamic frictional force acting on contact points of exploration robots is sufficiently large owing to the existence of higher gravity. Hence, the utilization of friction as the driving force, such as in the case of wheel mobility, is an appropriate method of facilitating movement. However, an asteroid-surface environment is very different from that of Mars. The characteristics of the environment include the existence of microgravity (10^{-6}~10^{-4}G) and uneven surfaces. On asteroid surfaces, if exploration robots do not actively push the surface, the frictional force acting on the robots is very small due to the microgravity environment of asteroids. Therefore, it is necessary for asteroid-exploration robots to use appropriate moving methods. Some examples of exploring robots include MINERVA [3], which was developed by JAXA, MASCOT [4] developed by European Space Agency (ESA) and German Aerospace Center (DLR) and Hedgehog [5] developed by Stanford University and the Jet Propulsion Laboratory at the National Aeronautics and Space Administration (NASA/JPL). All the aforementioned examples adopted the use of hopping mobility. Robots that use hopping mobility actively push the surface of the ground. Therefore, even if the robots are in a microgravity environment, a large frictional force acts on the robots. Therefore, hopping movement is an appropriate moving method for this application. These three robots have similar hopping mechanisms albeit with minor differences The hopping mobility allows for a high performance in leaping over obstacles and high traveling time efficiency. Moreover, the three robots have the advantage of a simplified structure in which their actuator is attached inside their body. However, the implementation of a soft-landing technique for such a robot is still challenging, and thus, the robot repeatedly rebounds on an asteroid surface until it comes to a stop. Therefore, factors affecting destination accessibility, such as the locomotion accuracy of the hopping robot involves uncertainties.

In this study, an analysis of the hopping and rebound-

Figure 1 : Process of Hopping and Rebounding

ing characteristics of a hopping robot such as MINERVA that is equipped with an internal torquer is performed using numerical simulations. Section 2 presents the dynamics models of hopping and rebounding. Section 3 presents the experiments for verifying the accuracy of these dynamics models. Section 4 presents the numerical simulations of the rebounding motion and the argument of the destination accessibility. In this study, as part of the destination accessibility analysis, the effects of the attitude and angular velocity of the robot at collision with the asteroid surface on the locomotion accuracy, traveling time, energy efficiency, and characteristics of leaping over obstacles are clarified.

2 DYNAMICS MODELING

The following two main dynamics models are used for simulating the motion of the robot: hopping and rebounding dynamics models. In this research, hopping means the torque applied by the robot torquer actively pushes the ground and the robot is pushed up by the reaction force. In contrast, rebounding means that the robot is pushed up owing to a collision between the robot and the ground after hopping. The process of hopping and rebounding is shown in Fig. 1.

2.1 Hopping

The dynamics model of the hopping robot is shown in Fig. 2. The robot can hop by using the reaction torque of the internal torquer that is attached to the center of gravity (CoG) of the robot. This research considers the case of a flat surface and a cubic robot. The robot applies a pushing force in the direction perpendicular to the line A shown in Fig. 2. The equation of the hopping motion of the robot is given as follows:

- Case1: The contact point does not slip

$$\begin{cases} m\dfrac{d^2x}{dt^2} = \dfrac{T}{r}\cos\beta \\ m\dfrac{d^2y}{dt^2} = \dfrac{T}{r}\sin\beta \end{cases} \tag{1}$$

$$\begin{aligned} I\frac{d^2\alpha}{dt^2} =& -T + r\cos\left(\alpha+\frac{\pi}{4}\right)\times\frac{T}{r}\sin\beta \\ &+ r\sin\left(\alpha+\frac{\pi}{4}\right)\times\frac{T}{r}\cos\beta \end{aligned} \tag{2}$$

- Case2: The contact point slips

$$\begin{cases} m\dfrac{d^2x}{dt^2} = \mu_d\dfrac{T}{r}\sin\beta \\ m\dfrac{d^2y}{dt^2} = \dfrac{T}{r}\sin\beta \end{cases} \tag{3}$$

$$\begin{aligned} I\frac{d^2\alpha}{dt^2} =& -T + r\cos\left(\alpha+\frac{\pi}{4}\right)\times\frac{T}{r}\sin\beta \\ &+ \mu_d r\sin\left(\alpha+\frac{\pi}{4}\right)\times\frac{T}{r}\sin\beta \end{aligned} \tag{4}$$

where m is the mass of the robot, I is the moment of inertia, g is the gravitational acceleration, μ_d is the dynamic friction coefficient, r is the length from the robot CoG to the contact point, T is the reaction torque exerted by the torquer, α is the attitude of the robot, and β is the angle between the pushing force vector of the robot and the ground. If the static friction coefficient $\mu = \infty$, i.e., the edge of the robot comes into contact with the ground and does not slip, the equation of hopping motion can be described using Eq. (1). In contrast, if $\mu \neq \infty$, the equation of hopping motion can be described using Eq. (1) or Eq. (3). In particular, in the case of $\mu < 1$, the equation can be described by Eq. (3). This paper targets only the case of $\mu < 1$. Hence, the hopping angle θ can be expressed as follows:

$$\theta = \tan^{-1}\frac{v_x}{v_y} = \tan^{-1}\mu_d \tag{5}$$

Moreover, from Eq. (3), it is clear that the contact point of the robot always slips while the torquer of the robot applies a torque. It is also clear that the pushing force of the robot becomes 0 when $T = 0$ or $\sin\beta = 0$. Therefore, the condition for which hopping is realized is either the torque is cancelled or $\alpha = 45°$. Here, a relationship between the angular acceleration and the torque obtained from Eq. (4) can be expressed as follows:

$$\frac{d^2\alpha}{dt^2} \propto T \tag{6}$$

Therefore, the time for hopping has the following relationship.

$$t \propto \frac{1}{\sqrt{T}} \tag{7}$$

Moreover, the reaction force experienced by the robot during hopping is proportional to T from Eq. 3. Thus, the translational impulse experienced by the robot during hopping can be expressed as follows.

$$F_x\Delta t \propto \sqrt{T} \tag{8}$$

$$F_y\Delta t \propto \sqrt{T} \tag{9}$$

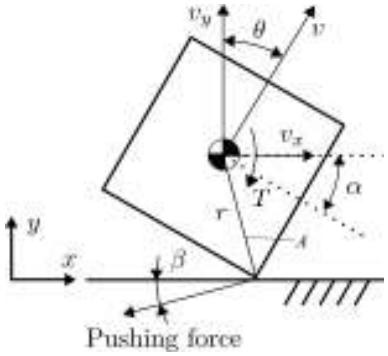

Figure 2 : Dynamics Model of Hopping

Therefore, the initial velocity can be expressed as follows.

$$v_x \propto \sqrt{T} \tag{10}$$

$$v_y \propto \sqrt{T} \tag{11}$$

2.2 Rebounding

The ground is modeled as comprising linear springs and dampers as shown in Fig. 3. In order to simulate the characteristics of the ground, the elastic constants used are $k_x = 5000$ [N/m] and $k_y = 10000$ [N/m] and the viscosity constants are $d_x = 5$ [Ns/m] and $d_y = 10$ [Ns/m]. Δx and Δy are the virtual penetration or displacement of the contact point along the x and y axis, respectively. The horizontal and normal contact forces N_x and N_y can be expressed as follows:

$$N_x = \begin{cases} k_1 \Delta x + d_1 v_x, & \text{if } v_x = 0 \\ \mu_d N_y, & \text{otherwise} \end{cases} \tag{12}$$

$$N_y = k_2 \Delta y + d_2 v_y \tag{13}$$

3 EXPERIMENTS

In this section, some experiments conducted for the verification of the dynamics models are presented.

3.1 Environment of Experiment

The environment considered for the experiment in order to verify the validity of the dynamics model of hopping is shown in Fig. 4. Moreover, the testbed is shown in Fig. 5. The testbed was fitted with a motor, air tanks, and air bearings under its body. The air tanks contained compressed air, and the robot blows air through its air bearings. Using these instruments, the robot can float against the stone plate and can move in the microgravity environment in

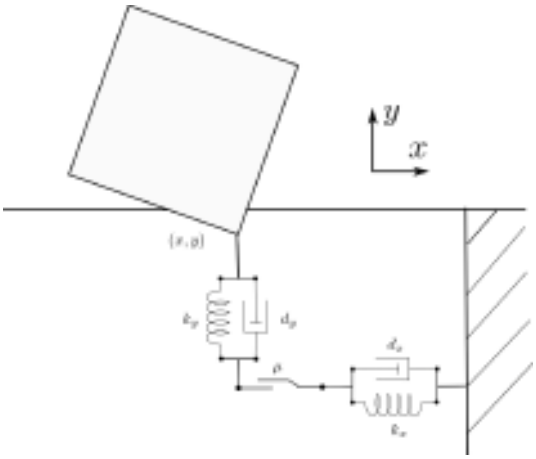

Figure 3 : Dynamics Model of Rebounding

2D. The users of this environment can change the acceleration of gravity by tilting the stone plate. The vertical and horizontal dimensions testbed were 15 *times* 15 cm, and its weight was 4.3 kg. The edges of this testbed were fabricated using acrylonitrile butadiene styrene copolymer (ABS) in a 3D printer. The testbed also had a microcontroller Arduino, which is connected operator's PC by using XBee. Using this connecting system, the operators can control the rotational frequency of the motor. The position of the testbed is recorded using a motion tracking system.

3.2 Hopping Experiment

The hopping experiment was executed using the aforementioned environment. The process of this experiment is as follows:

1. Setting the attitude of the testbed α to 0 and being settle on the simulated surface
2. The motor in the testbed is rotated for a certain amount of time.
3. The testbed hops.

The conditions of the hopping experiment are as follows:

- The acceleration of gravity is 5.0×10^{-4}G .
- The time of applied torque is 0.3 s (limit of the motor).
- The materials used for contact point of the robot are ABS and rubber.
- The frequency of rotation of the motor is 30 Hz.

In the case of the hopping motion, the appearance of the contact point comparing two different types of materials is shown in Figs. 7 and 8 ($t = 0$ is the time at which the torque is applied). These figures ilustrate the view from

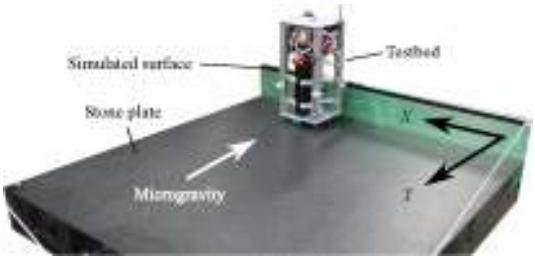

Figure 4 : Environment of Experiment

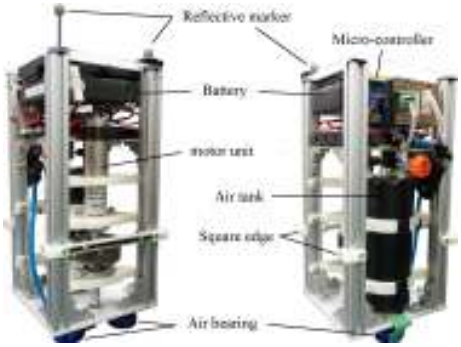

Figure 5 : Air-floating Testbed

above the testbed, and the schematic is shown in Fig. 6. Figures 7 and 8 illustrate the cases of ABS and rubber, respectively. Even if the material changes, i.e., the friction coefficient changes, the edge of the testbed always slips between the time of torque application and that of hopping. In general, the friction coefficient of rubber is 1 or less. Thus, this result is suitable for the dynamics model. The attitude of hopping is almost 40° and 30°, respectively, when the material is ABS and rubber. This is because the CoG of the testbed is not located at its geometric center, and the motor is not located at the CoG; moreover, the applying time of torque reaches 0.3 s before the testbed hops.

The position of the geometric center of the testbed when the frequency of rotation is 30 Hz and the material is ABS is shown in Fig. 9. The position of the geometric center of the testbed when the frequency of rotation is 30 Hz and the material is rubber is shown in Fig. 10. Here, the position of the geometric center is almost that same as that of the CoG. From these figures, the initial velocity of the testbed during hopping is derived. As shown in Fig. 9, the translational velocities (v_x, v_y) are 0.013851 m/s and 0.060575 m/s, respectively. As shown in Fig. 10, the translational velocities are 0.036832 m/s and 0.051758 m/s, respectively. Therefore, the ratio of the translational velocities v_x/v_y is 0.23 and 0.714 for ABS and rubber, respectively. Here, on considering the dynamic friction coefficient of ABS and rubber as 0.2~0.3 and 0.6~0.7, respectively, the resultant initial velocity is suitable for the dynamic model.

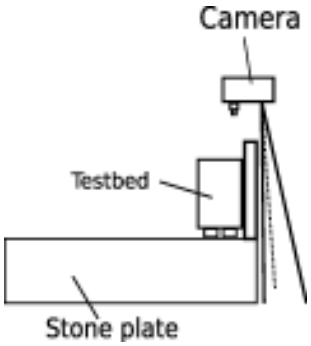

Figure 6 : Recording Position

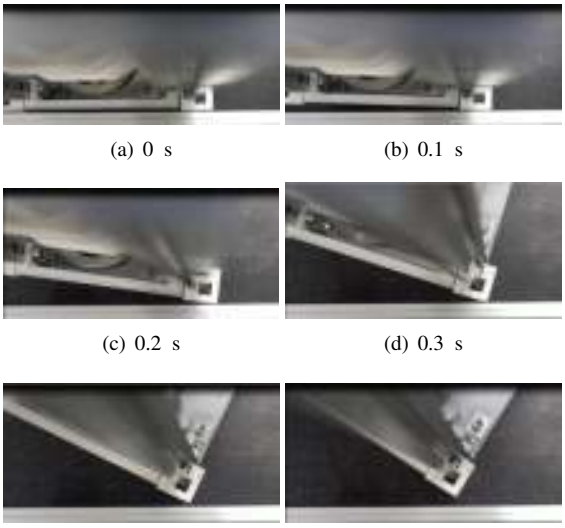

(a) 0 s (b) 0.1 s

(c) 0.2 s (d) 0.3 s

(e) 0.4 s (f) 0.5 s

Figure 7 : State of Contact Point During Hopping (Material of Contact Point: ABS)

4 SIMULATION ANALYSIS

4.1 Rebounding Simulation

In this study, the dynamics calculation was performed using MATLAB, and the simulation results are visualized using Gazebo to obtain more reliable simulation results.

4.1.1 Effect of attitude angle at collision

At first, an effect of the attitude angle α of the robot when focusing on the translational velocity after the rebound was analyzed. The analysis conditions are as follows:

- α = 10, 20, 30, and 40 [∘]
- μ_d = 0.1, 0.2, $\cdots$, 0.8, and 0.9 [-]
- v_x/v_y = 0.1, 0.2, $\cdots$, 0.8, and 0.9 [-]

This simulation was performed with a total of 324 conditions. The image of this simulation is shown in Fig. 11.

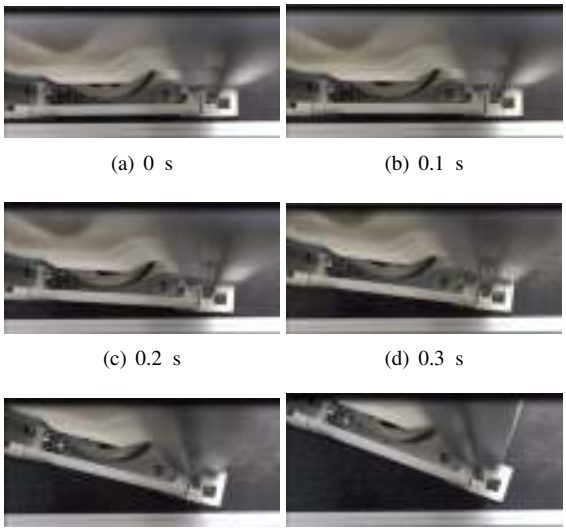

(a) 0 s (b) 0.1 s

(c) 0.2 s (d) 0.3 s

(e) 0.4 s (f) 0.5 s

Figure 8 : State of Contact Point During Hopping (Material of Contact Point: Rubber)

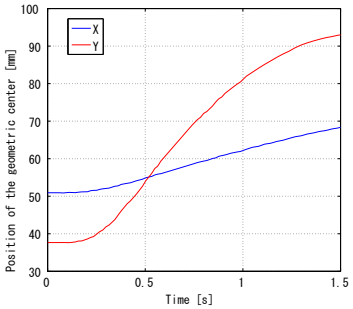

Figure 9 : Position of Geometric Center of Testbed (30 Hz, ABS)

The resulting relationship between the ratio of the horizontal velocity before and after the collision and μ_d is shown in Figs. 12, 13, and 14, where the velocity ratios are $v_x/v_y = 0.1$, $v_x/v_y = 0.5$, and $v_x/v_y = 0.9$ respectively. The ratio in these figures are negative because of a calculation error in this simulation. This result confirms that the rate of decrease of the post-collision velocity becomes smaller with an increase in α. This is because the robot's angular velocity ω after the collision decreases in proportion to the increase in the moment M of the frictional force as α approaches 40°. Therefore, the translation momentum after the collision increases with an increase in α, where the given impulse is constant without a collision attitude change. This characteristic was observed for the various values of v_x/v_y. Here, M is given by the following equations.

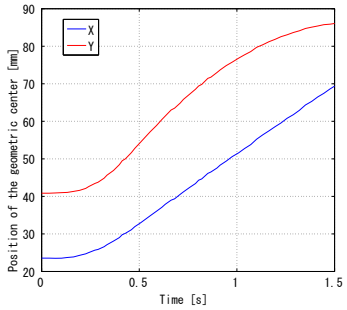

Figure 10 : Position of Geometric Center of Testbed (30 Hz, Rubber)

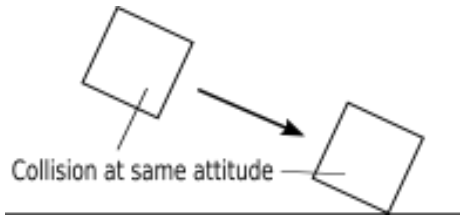

Figure 11 : Image of Collision without Angular Velocity

If $0° \leqq \alpha \leqq 45°$,

$$M = -N_x r \cos\left(\alpha + \frac{\pi}{4}\right) + N_y r \sin\left(\alpha + \frac{\pi}{4}\right) \tag{14}$$

If $45° \leqq \alpha \leqq 90°$,

$$M = -N_x r \cos\left(\alpha + \frac{\pi}{4}\right) - N_y r \sin\left(\alpha + \frac{\pi}{4}\right) \tag{15}$$

4.1.2 Effect of rotational velocity at collision

Next, the effect of a constant ω on the translation speed after the collision was analyzed. The analysis conditions are as follows:

- ω = -1.0, -1.1, $\cdots$, -1.8, and -1.9 [rad/s]
- α = 10, 20, 30, and 40 [$\circ$]
- v_x/v_y = 0.3, 0.5, and 0.7 [-]

This simulation was performed with a total of 120 conditions. The image of this simulation is shown in Fig. 15.

The resulting relationship between the vertical velocity ratio before and after the collision and v_x/v_y are shown in Figs. 17, 18, and 19, where ω is -1.3 rad/s, -1.6 rad/s, and -1.9 rad/s, respectively. From this result, it is found that the vertical velocity ratio becomes larger than 1 in the case that α is 30° or 40° at the collision. Here, the normal force N_y can be expressed as follows:

$$\begin{aligned} N_y &= k_2 \Delta y + d_2 \left\{ v_y + r\omega \sin(\beta) \right\} \\ &= k_2 \Delta y + d_2 \left\{ v_y + r\omega \sin\left(\frac{\pi}{4} - \alpha\right) \right\} \end{aligned} \tag{16}$$

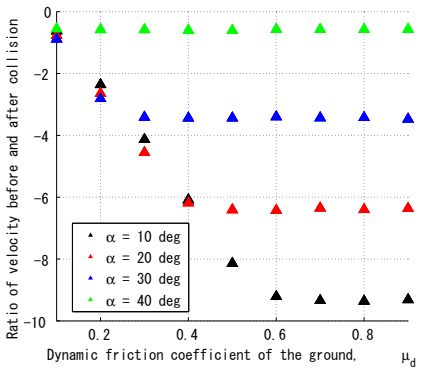

Figure 12 : Ratio of Horizontal Velocity Before and After Collision (Without Angular Velocity, $v_x/v_y = 0.1$)

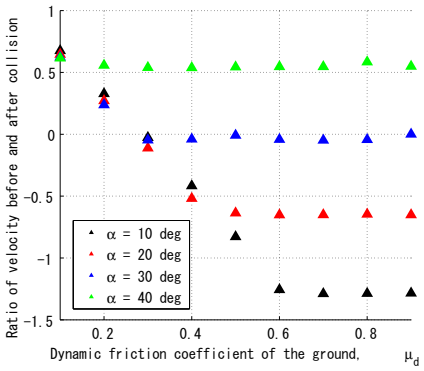

Figure 13 : Ratio of Horizontal Velocity Before and After Collision (Without Angular Velocity, $v_x/v_y = 0.5$)

As shown in Eq. (16), N_y reaches a maximum value when α is almost 0°. In addition, as shown in Eq. (15), M reaches a minimum value when α is 45°. Therefore, in order to maximize the translational velocity after the collision, it is necessary to increase N_y and reduce M. In this case, the most appropriate value of α is within 30°~40°. This appropriate range also does not depend on ω.

4.2 Destination Accessibility

The vertical and horizontal impulse, $F_y\Delta t$ and $F_x\Delta t$, experienced by the robot at the collision are $mv_y \leqq F_y\Delta t \leqq 2mv_y$ and $-2\mu_d mv_y \leqq F_x\Delta t \leqq -\mu_d mv_y$ in accordance with the linear spring–damper model. The horizontal impulse during hopping is $\mu_d mv_y$, and thus, the velocity of the contact point becomes 0 when the robot collides with the ground surface. The image of this phenomenon is shown in Fig. 16. The experiment for verifying this phenomenon is conducted with the environment shown in Fig. 4. The experiment results confirmed that the aforementioned phenomenon occurred. In addition, the testbed rotated because the testbed experienced the negative torque of the dynamic friction force at the collision.

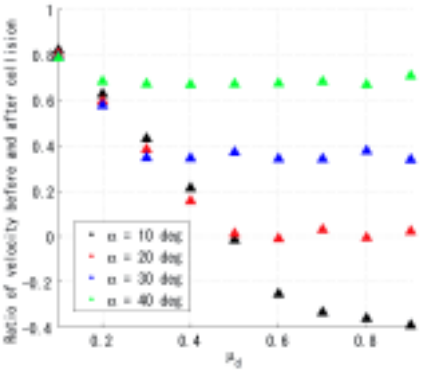

Figure 14 : Ratio of Horizontal Velocity Before and After Collision (Without Angular Velocity, $v_x/v_y = 0.9$)

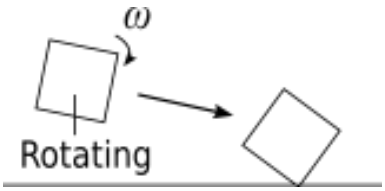

Figure 15 : Image of Collision with Angular Velocity

4.2.1 Moving mode (i)

In the case of moving mode (i), it is assumed that α can be maintained at 0° at the collision through active control of the torquer before the collision. By adopting this mode, the horizontal velocity of the robot ' s CoG after the collision is almost 0. Consequently, the robot can accurately reach and stay near a destination point in a single hop (see Fig. 20(a)). In contrast, if the distance between the current position of the robot and the destination is very large, the hopping velocity of the singe hop locomotion could exceed the escape velocity for the target body. Therefore, the robot should use multiple short-distance hops in a practical situation. Furthermore, moving mode (i) is inefficient from the viewpoint of energy consumption.

4.2.2 Moving mode (ii)

In the case of moving mode (ii), it is assumed that α is approximately 40° at the collision. In this mode, the horizontal velocity of the robot decays in small amounts owing to the collision. Thus, the robot can move more efficiently and faster than that using mode (i) (see Fig. 20(b)).

4.2.3 Moving mode (iii)

In the case of moving mode (iii), it is assumed that the rotating robot collides with the ground surface. In this mode, the robot can possess a larger vertical velocity owing to the collision than that before the collision. This suggests that the robot can leap over obstacles more efficiently by actively utilizing the rebound (see Fig. 20(c)).

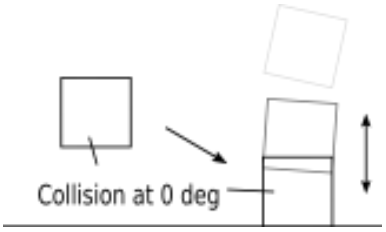

Figure 16 : Image of Collision at 0°

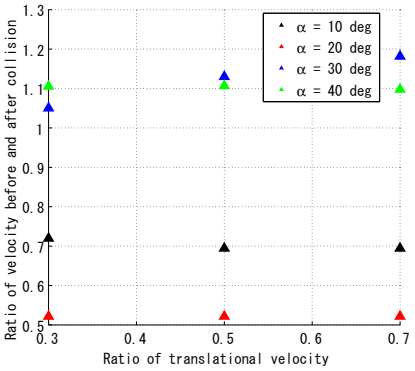

Figure 17 : Ratio of Vertical Velocity Before and After Collision (With Angular Velocity, $\omega = -1.3$)

4.2.4 Comparison

Using the results of the three moving modes, the destination accessibility of each mode is summarized in Tab. 1. Based on this comparison, it can be inferred that the hopping robot can adjust its mobility performance by simply controlling the robot's attitude and angular velocity at collision. This comprises the control of momentum transfer at the collision. In practical applications, the hopping mode should be selected such that the robot ' s mission requirements are satisfied.

5 CONCLUSION

In this study, the effects of various collision conditions of a hopping robot on its rebounding performance are analyzed to obtain improved destination accessibility on an asteroid with a microgravity environment. The results confirmed that the robot can change the ratio of the translation and angular momentum after the rebound by controlling the robot's attitude and angular velocity at collision. Therefore, this study suggests the possibility of the

Table 1 : Destination Accessibility of Moving Modes

Mode	Accuracy	Time	Efficiency	Leaping
(i)	✓			
(ii)		✓	✓	
(iii)				✓

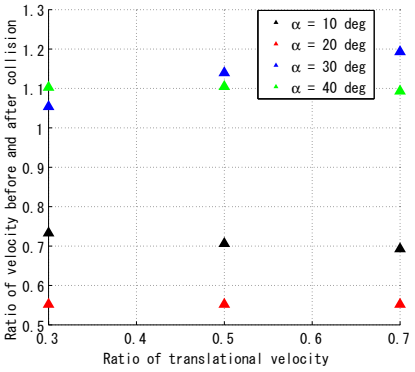

Figure 18 : Ratio of Vertical Velocity Before and After Collision (With Angular Velocity, $\omega = -1.6$)

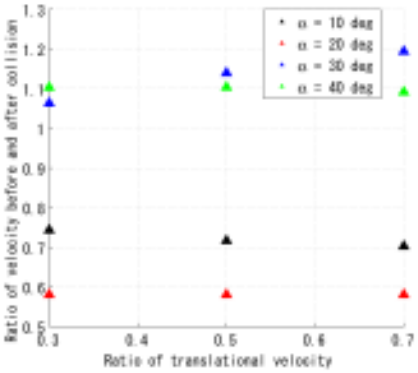

Figure 19 : Ratio of Vertical Velocity Before and After Collision (With Angular Velocity, $\omega = -1.9$)

achievement of a more adaptive hopping mobility to meet requirements of accuracy, efficiency, or safety.

References

[1] J. Saito et al., Detailed Images of Asteroid 25143 Itokawa from Hayabusa, *Science*, Vol. 312, pp. 1341-1344, 2006.

[2] H. Kuninaka et al., Hayabusa Asteroid Explorer Powered by Ion Engines on the way to Earth, *Proceedings of the 31st International Electric Propulsion Conference*, #267, 2009.

[3] T. Yoshimitsu et al., Micro-Hopping Robot for Asteroid Exploration, *Acta Astronautica*, Vol. 52, pp. 441-446, 2003.

[4] M. Lange et al., MASCOT - Structures Design and Qualification of an " Organic " Mobile Lander Platform for Low Gravity Bodies, *Proceedings of the 13th European Conference on Space Structures, Materials and Environmental Testing*, vol. SP-727, 2014.

[5] B. Hockman et al., Design, Control, and Experimentation of Internally-Actuated Rovers for the Exploration of Low-Gravity Planetary Bodies, *Journal of Field Robotics*, vol. 34, pp. 5-24, 2016.

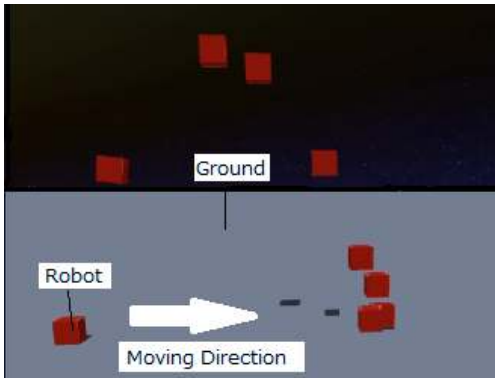

(a) Mode (i)

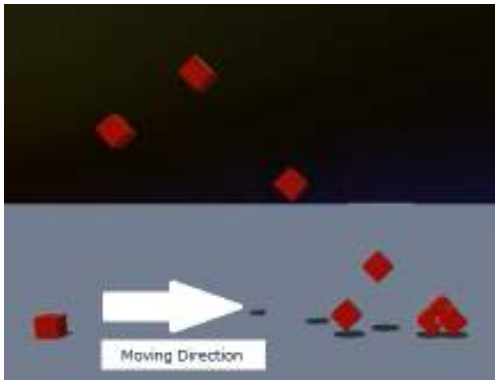

(b) Mode (ii)

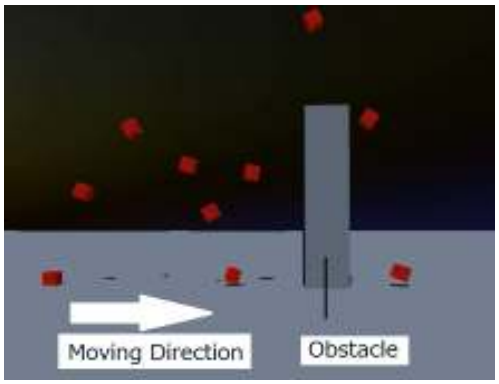

(c) Mode (iii)

Figure 20 : Result of Bound Simulation